12-15-1997

Large-Scale Estimation of Transport from the Pacific to the Indian Ocean

James T. Potemra
University of Hawaii

Roger Lukas
University of Hawaii

Gary T. Mitchum
University of South Florida, mitchum@usf.edu

JOURNAL OF GEOPHYSICAL RESEARCH, VOL. 102, NO. C13, PAGES 27,795–27,812, DECEMBER 15, 1997

Large-scale estimation of transport from the Pacific to the Indian Ocean

James T. Potemra and Roger Lukas

Department of Oceanography, University of Hawaii, Honolulu

Gary T. Mitchum

Department of Marine Science, University of South Florida, St. Petersburg

Abstract. The objective of this model-data intercomparison is to determine the feasibility of deriving an useful index for fluctuations in the Pacific to Indian Ocean throughflow volume transport. Due to insufficient direct observations and the present limitations in numerical models, accurate estimation of variations in the throughflow transport on seasonal to interannual timescales is not yet possible; however, an index based on weighted, monthly mean sea level anomalies in different regions of the western Pacific and eastern Indian Oceans is presented. Numerical model results and sea level from the TOPEX/POSEIDON altimeter show that the large-scale pressure gradient forcing of the throughflow is controlled by the Pacific Ocean side on interannual timescales, and by a combination of Indian Ocean and Pacific Ocean processes on seasonal to annual timescales. The model throughflow is maximum in boreal summer (11 Sv) and minimum in boreal winter (4 Sv) with a 9-year mean of 7.4 Sv. These values are within the range of various estimations of throughflow transport, and they agree in phase. Of the 7.4 Sv model transport, almost 1.8 Sv is due to direct, local wind forcing (based on Ekman calculations). Interannual fluctuations from El Niño-Southern Oscillation activity are associated with increases in throughflow transport during cold events and decreases in transport during warm events. Using empirical orthogonal function analysis and results from previous studies, an index of the throughflow variability is developed using model sea level and model transport. Sea level in four regions is found to be sufficient to index the model throughflow variations: south of Java, northwest of Australia, in the Pacific warm pool and off the coast of the Philippines. A regression technique applied to the model sea level at these locations yields an index which correlates with the model throughflow at 0.83. The same weights applied to sea level in similar regions from the TOPEX/POSEIDON altimeter correlate with the model throughflow transport at a level of 0.78.

1. Introduction

The existence of net flow from the Pacific Ocean to the Indian Ocean through the Indonesian seas has been known since the seminal work of *Wyrtki* [1961]; however, the volume transport and its variability still have not been adequately quantified [*Godfrey,* 1996]. It is thought that this Indonesian throughflow (ITF) has important climate implications both regionally and globally. Thus it is desirable to not only quantify the ITF and its variability, but to monitor it in the long term. This paper describes a remote sensing approach to a sea-level-based index of ITF transport.

Paper number 97JC01719.
0148-0227/97/97JC-01719$09.00

Wyrtki [1987] first proposed such an index using in situ observations, noting that the driving force for the ITF is provided by the pressure head between the western equatorial Pacific and the region (here called the Indo-Australian Basin) of the eastern Indian Ocean to the north of Australia and west of the Timor Sea. He estimated this driving force by using the mean dynamic height difference (16 dyn cm relative to 1000 dbar) between the far western equatorial Pacific and the Indo-Australian Basin using historical hydrographic data [*Levitus,* 1982].

To estimate the variability of the ITF, the pressure difference between the Pacific and Indian Oceans was inferred from the observed monthly sea level anomalies at coastal tide gauge stations at Davao, Mindanao Island (Philippines), and at Darwin, Australia. It should be noted that *Wyrtki* [1987] suggested that sea level variations along the south coast of Java would have

been more suitable than those at Darwin for capturing the variability in the driving force, due to the vigorous upwelling which occurs there during the southeast monsoon. However, such observations were not available. The resulting sea level index for the ITF ranged from -9 to 46 cm during the period 1977-1984, with an average annual cycle of 9 to 23 cm. The phase of the annual cycle compared well with the numerical model results of *Kindle et al.* [1987, 1989], but the interannual variations were quite different, and *Wyrtki* [1987] did not attempt to calibrate the sea level index in terms of volume transport. Interannual variability of the sea level index did not show a good correspondence with model El Niño-Southern Oscillation (ENSO) events, which *Wyrtki* [1987] believed was due to large-scale convergence patterns in the wind field associated with ENSO, with the result that sea level was affected over a broad area without substantially affecting the pressure head.

Clarke and Liu [1994] provided a basis for understanding the lack of an ENSO signal in *Wyrtki's* [1987] sea level index, explaining that the sea level patterns associated with the annual cycle and those associated with interannual variations are quite different and that the simple sea level difference between Davao and Darwin cannot adequately represent both timescales. In particular, these off-equatorial coastal sites are only indirectly related to the equatorial waveguide variations in the Indian and Pacific Oceans associated with ENSO. Because of the limited number of relevant tide gauge sites with long time series, there was not much prospect of developing a better sea level index.

Now, with the availability of high quality satellite altimetry data provided by the TOPEX mission, the possibility exists to develop a more accurate representation of the pressure head which drives the ITF and to monitor it as long as such remotely sensed sea level is available. In this study, a numerical model is used in conjunction with the TOPEX data to identify regions of sea level variability on annual and interannual timescales. Due to complex boundaries and coupled processes that occur in this region, and the lack of observations for calibration and validation, numerical models are not yet capable of reproducing verifiable, accurate throughflow variations. It is suggested here, however, that a model be used to identify key regions that are thought to control the pressure-driven aspect of the throughflow. Once these regions have been identified, the model index can be validated against its own throughflow transport variability. A multiple linear regression (MLR) technique is used to optimally fit the sea level at these locations to the model throughflow transport. The weights determined from the MLR fit are then applied to the TOPEX data at similar locations. In the following section, the strategy for developing the throughflow transport index and the data used are described. Next, the throughflow variability from the model is detailed. The derivation of the index is then outlined and applied to the model and TOPEX sea level fields. Finally, some discussion on future work is presented.

1.1. Strategy for Sea-Level-Based Monitoring

Our primary objective is to develop a sea-level-based index of the ITF volume transport for use in ongoing monitoring of this important ocean circulation feature and for use in understanding the ITF variability in relation to the interannual variations of the western Pacific warm pool. An important issue is to determine which fraction of the ITF transport is attributable to large-scale pressure gradients and which portion is due to directly wind-driven transport. Neither *Wyrtki* [1987] nor *Clarke and Liu* [1994] addressed the directly wind-forced component of transport variation, which may be important on both annual and interannual timescales. Even an optimal sea level index cannot monitor the directly wind-driven component of ITF transport variations.

There are relatively few direct measurements of ITF transport [e.g., *Fieux et al.*, 1994, 1996; *Molcard et al.*, 1994], and there are no such time series of sufficient duration to address interannual variability. The longest time series of estimated ITF transport is that of *Meyers et al.* [1997] using expendable bathythermograph (XBT) temperature profiles, historical temperature and salinity relationships and geostrophy along a ship route between Australia and Indonesia. While this time series is several years long, it has a relatively short overlap with the TOPEX/POSEIDON data. There are also issues of the reference level and barotropic flow. Until direct time series measurements of transport are sufficiently long, a "bootstrap" approach is necessary. Below, we describe the strategy that we are pursuing.

The starting point in the approach to an altimetric sea level index for the ITF transport is to identify an ocean general circulation model (OGCM) which (1) has physics appropriate to the problem, (2) is large in scale (has a domain with tropical and extratropical Pacific and Indian Oceans), (3) has adequate resolution, and (4) is forced by realistic winds. The *Semtner and Chervin* [1988, 1992] Parallel Ocean Climate Model (POCM) was deemed adequate, as is described below in section 1.3.

Once the dominant patterns of sea level variability associated with significant ITF variability are indentified within the model, sea level at key locations (averaged over some region to reduce noise) is then correlated with simultaneous model ITF transport to obtain least squares estimates of their weight in determining the pressure head. The model in this study needs to have accurate physics, but the performance of the model in the Indonesian seas need not be exact. Following *Wajsowicz* [1996], the throughflow can be viewed as an electric circuit where flow through straits is analogous to resistors. Here the interest is in the total resistance supplied by all the straits.

Once the sea level index has been developed within the POCM framework, the scheme is applied directly to TOPEX/POSEIDON observations. Ultimately, it will be desirable to independently test the skill of the sea-level-based ITF index by comparison against simultaneous transport observations. It may also be necessary to include in situ sea level in order to capture the amplitude maxima that frequently occur along coasts where the altimeter errors are relatively large.

1.2. TOPEX/POSEIDON Altimetric Observations

The TOPEX/POSEIDON satellite carries a radar altimetry system specifically designed to measure sea level variability. The satellite was launched in August 1992 and has returned very high quality data since October 1992 with relatively few gaps. A variety of data processing procedures must be performed to the raw data stream [*Fu et al.*, 1994], resulting in sea level height variability which has an estimated average accuracy of 4-5 cm [*Mitchum*, 1994]. Errors are significantly higher in areas where tidal models are not accurate enough to eliminate aliasing by unresolved tidal variability, such as on the continental shelf of northwest Australia and within the Indonesian seas. Hopefully, future improvements in tidal models will make this point mute. Observations are available along the satellite ground tracks (see Figure 1) at intervals of 10 days.

1.3. The Parallel Ocean Climate Model

The *Semtner and Chervin* [1988, 1992] POCM is based on a multilevel, primitive equation formulation, and it parameterizes vertical mixing by a Richardson number scheme. The version used here has a mean 0.4° resolution (Figure 2) and 20 vertical levels. A complete description of the model parameters is given by *Stammer et al.* [1996].

When the prescribed horizontal eddy viscosity is sufficiently small, the mean horizontal grid spacing of 0.4° allows for explicit representation of instabilities that mix momentum, heat, salt, and other processes. In these cases, the model permits the existence of large-scale (100 km) eddies. The model was forced with daily European Centre for Medium-Range Weather Forecasts (ECMWF) 10 m winds for the period between January 1987 and December 1995, with prescribed surface heat fluxes [*Barnier et al.*, 1995] treated as a restoring force to climatological [*Levitus et al.*, 1994a,b] SST. This model has explicit free surface height variability and contains adequate horizontal and vertical resolution for the large-scale aspects of the ITF. The model has a maximum depth of 6000 m and uses an approximation of the actual bathymetry corresponding to the model resolution.

Many of the passages into the Indonesian seas are resolved in the POCM, with the exception of the Lombok Strait (between Lombok and Bali), which is only one

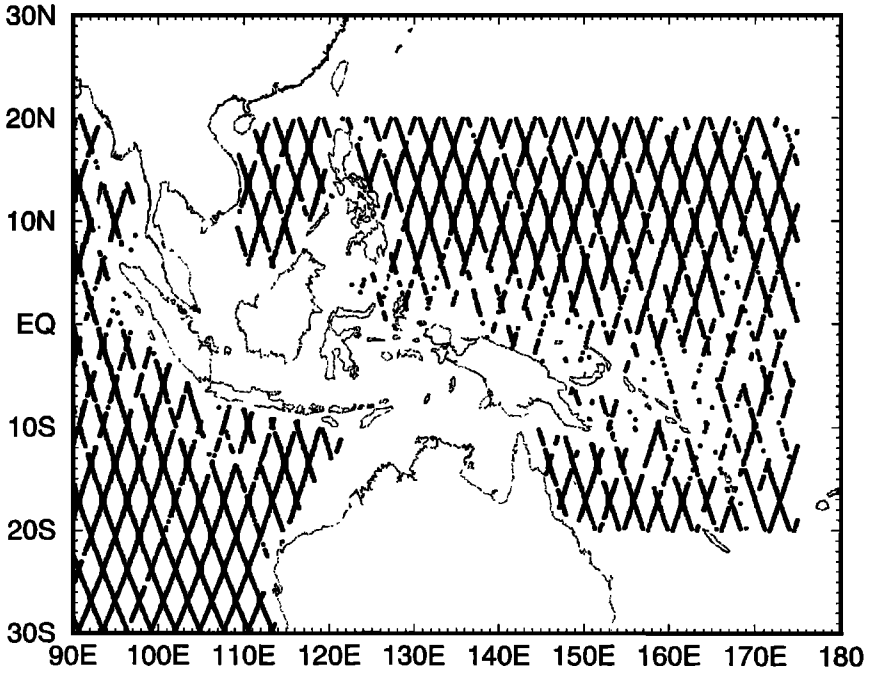

Figure 1. Regional map showing locations of TOPEX/POSEIDON observations used in this study, illustrating the ground track coverage. Gaps are in areas where the estimated noise/signal ratio is too high to be useful, largely due to poor tidal modeling or lack of useful observations due to rain.

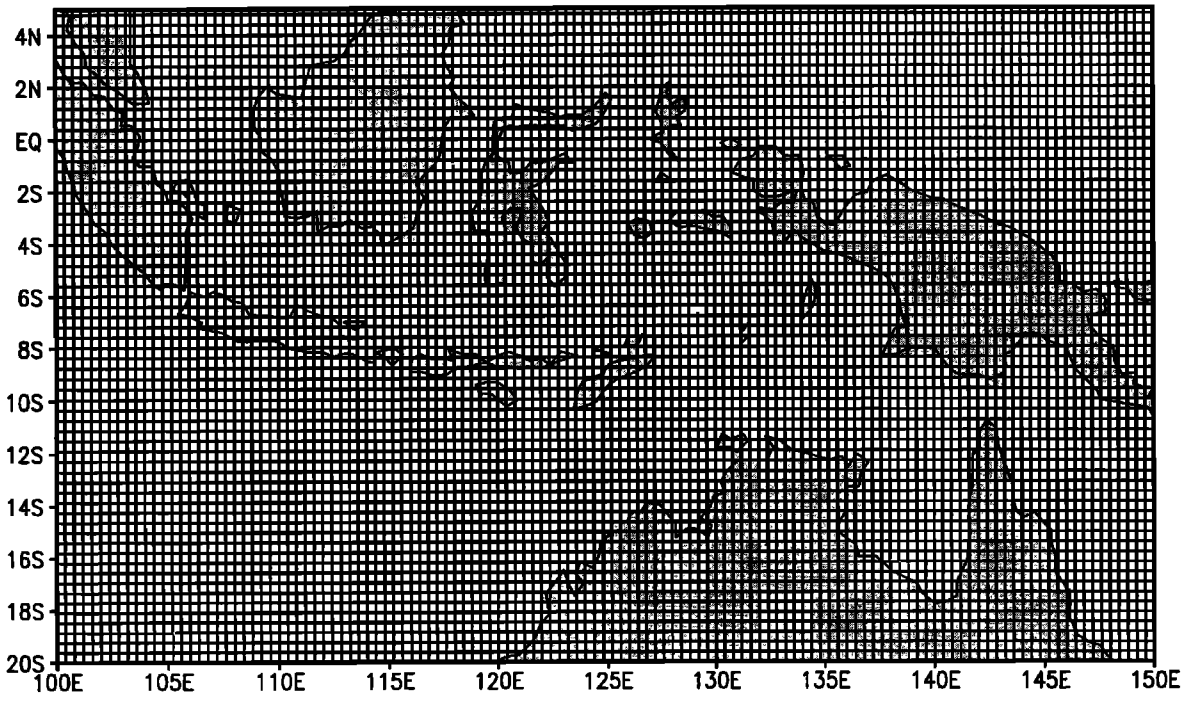

Figure 2. *Semtner and Chervin* [1992] model grid (surface layer) in the Indonesian seas. Shaded grid cells are land, while open grid cells represent ocean. Actual land outlines are shown by irregular black lines.

grid point wide. Its contribution to the ITF [*Murray and Arief,* 1988] is not resolved in this model. Additionally, the model Torres Strait (between Australia and New Guinea) is unrealistically deep (50 m) in the model. The POCM cannot address the controlling physics within the narrow straits and channels of the interior Indonesian seas. For example, it does not include the important influence of the very strong tidal mixing within the Indonesian seas [*Ffield and Gordon,* 1992].

2. Throughflow Variability

2.1. Sea Level Variability

In Figure 3 the wind climatology for the region and the POCM surface current streamlines are shown for the southeast monsoon and the northwest monsoon. Sea level differences between these extremes are largest in the Indo-Australian Basin and the South China Sea, while changes in the western equatorial Pacific are relatively small, especially near the western boundary. However, the surface flows in the western equatorial Pacific show a complete reversal of the zonal flow at the extremes of the monsoon (Figure 3). Such a flow reversal is also seen in the Indo-Australian Basin, though the flows there are largely meridional. These monsoonal surface current variations suggest the importance of Ekman transports for the annual cycle.

Model sea level has been favorably compared to observations using tide gauge data on a global scale [*Tokmakian,* 1996]. Here comparisons will be made only at locations of interest for this study. One such comparison is via empirical orthogonal function (EOF) decomposition of the model sea level field and the TOPEX altimeter data. This serves both as a check of large-scale model sea level and also to identify regions of variability in the sea level field that should be incorporated into the ITF index.

Ten-day output from the POCM for 1993 and 1994 (coincident with the TOPEX/POSEIDON mission) were compared via separate EOF analyses. Plate 1 shows the first three EOFs from the POCM and the altimeter. The first two EOFs reproduce the annual cycle in both the model and altimeter records and account for almost 40% of the variance in each. Similarities in both the time series and spatial patterns can be seen. Regions exhibiting the most variability appear to be the western Pacific warm pool, the southern coasts of Sumatra and Java, the west coast of Australia, and the southern subtropical Indian Ocean. The time series have correlation coefficients of 0.97 (POCM EOF 1 to TOPEX EOF 2) and 0.71 (POCM EOF 2 to TOPEX EOF 1) at one month lag.

The third EOFs account for 9% of the total variance in both the model and the altimeter signal. This EOF shows the difference between records for the two years, with large negative amplitudes during 1993 and positive values during 1994 which coincide with known ENSO activity. The POCM and TOPEX spatial patterns match fairly well, and the two time series have a

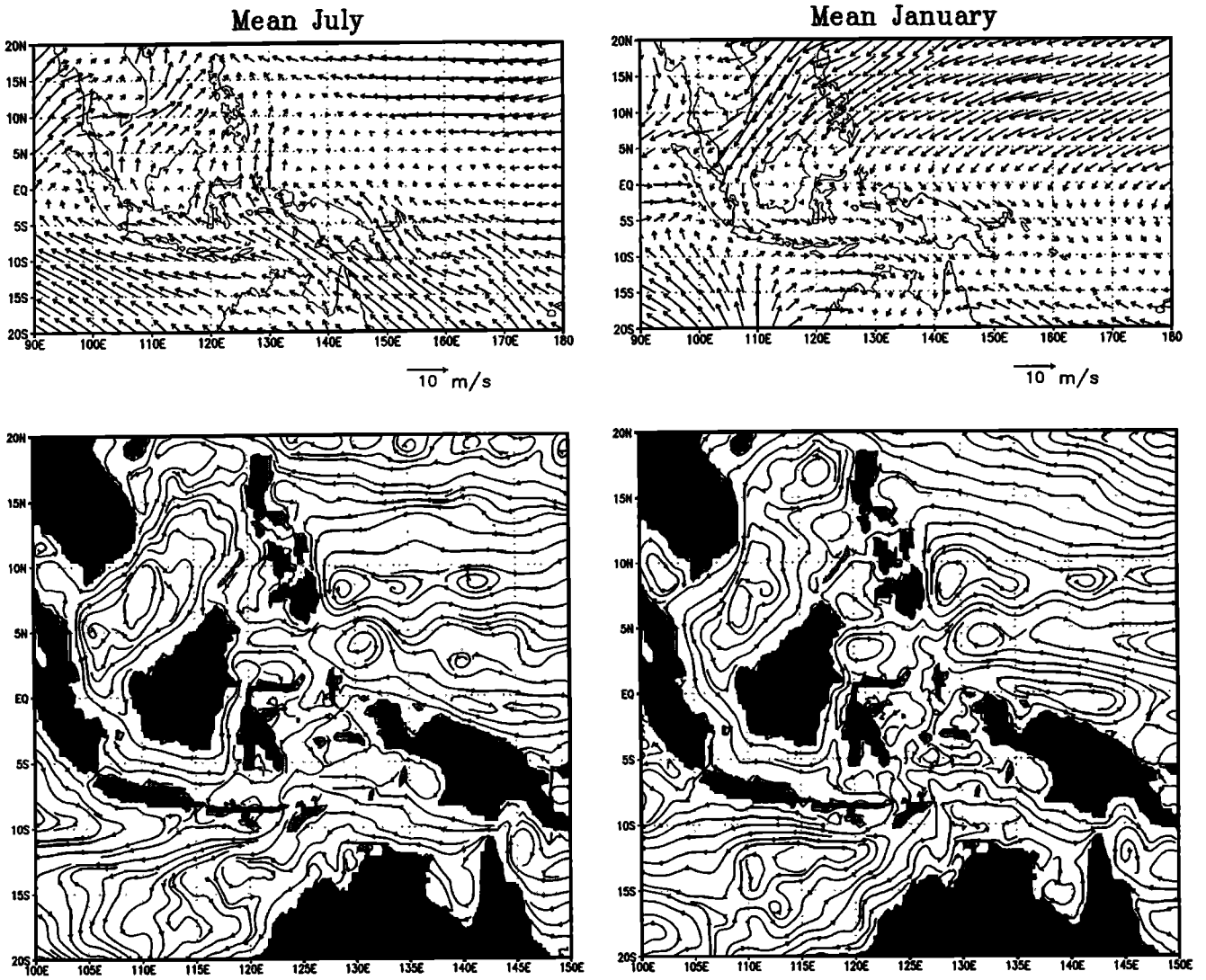

Figure 3. Mean wind and ocean circulation in the ITF region. (top) Mean ECMWF 10 m winds. A scale is given at the lower right of each panel. (bottom) Mean POCM velocity streamlines for the top 100 m of the model (four levels). The left side of each is the mean July and the right side is the mean January (for the wind, the mean is from 1985 through 1995, and for the velocity, the means are taken from 1987 through 1995).

maximum correlation of 0.76 at 1 month lag. Most variability is seen in the western Pacific warm pool, off the west coast of Australia, and along the southern coast of Sumatra and Java. The western Pacific and Australia are in phase with each other and out of phase with the Indonesian signal, consistent with the results of *Wyrtki* [1987] and *Clarke and Liu* [1994].

The EOF spatial patterns not only show an agreement between model and remote observations, but also serve to identify regions of sea level variability that could be used for the ITF index. In this case, the key regions seem to be the western Pacific warm pool, the southern coasts of Sumatra and Java, and the northwestern Australian coast. It would be reasonable, therefore, to base the ITF index on a combination of sea level signals from at least these locations.

2.2. Analysis of Model Throughflow

Given that the POCM captures significant aspects of the dominant modes of sea level variability, the next step is to develop a sea level index for the model ITF. This requires an understanding of the temporal and vertical structure of the ITF and ultimately the dynamics controlling the ITF variability. For this work, the flow in each strait need not be accurate, as long as the total net throughflow is and that storage of water in the region is not an issue. The flow through each strait and the total sum are therefore outlined here.

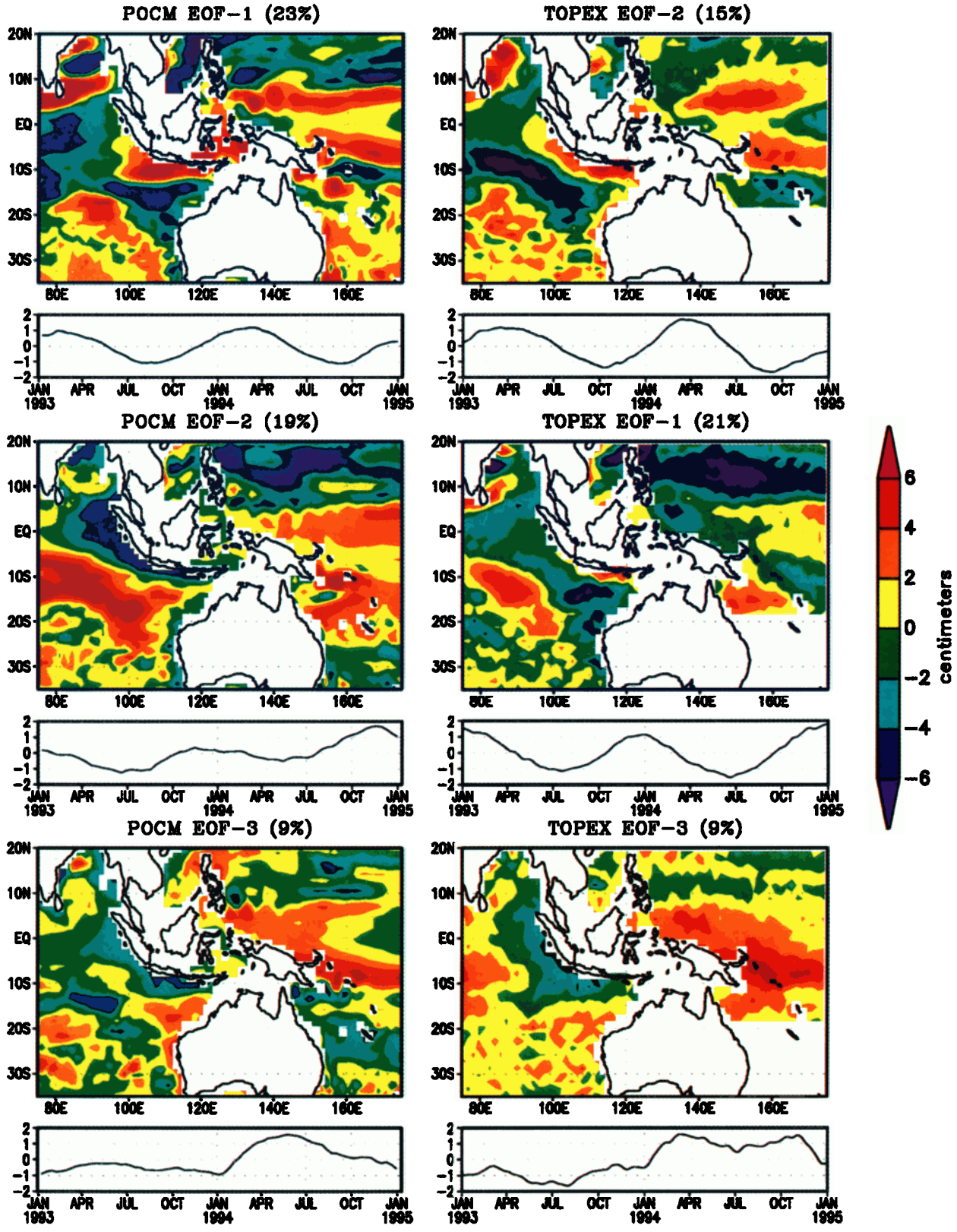

Plate 1. (left) First three EOFs of POCM free surface elevation and (right) the TOPEX/POSEIDON altimetric sea level height, for the period January 1993 through December of 1994. The scale for the spatial patterns is given on the right (in centimeters), and the corresponding time series is given below each EOF map. The vertical placement was chosen to match temporal-spatial patterns.

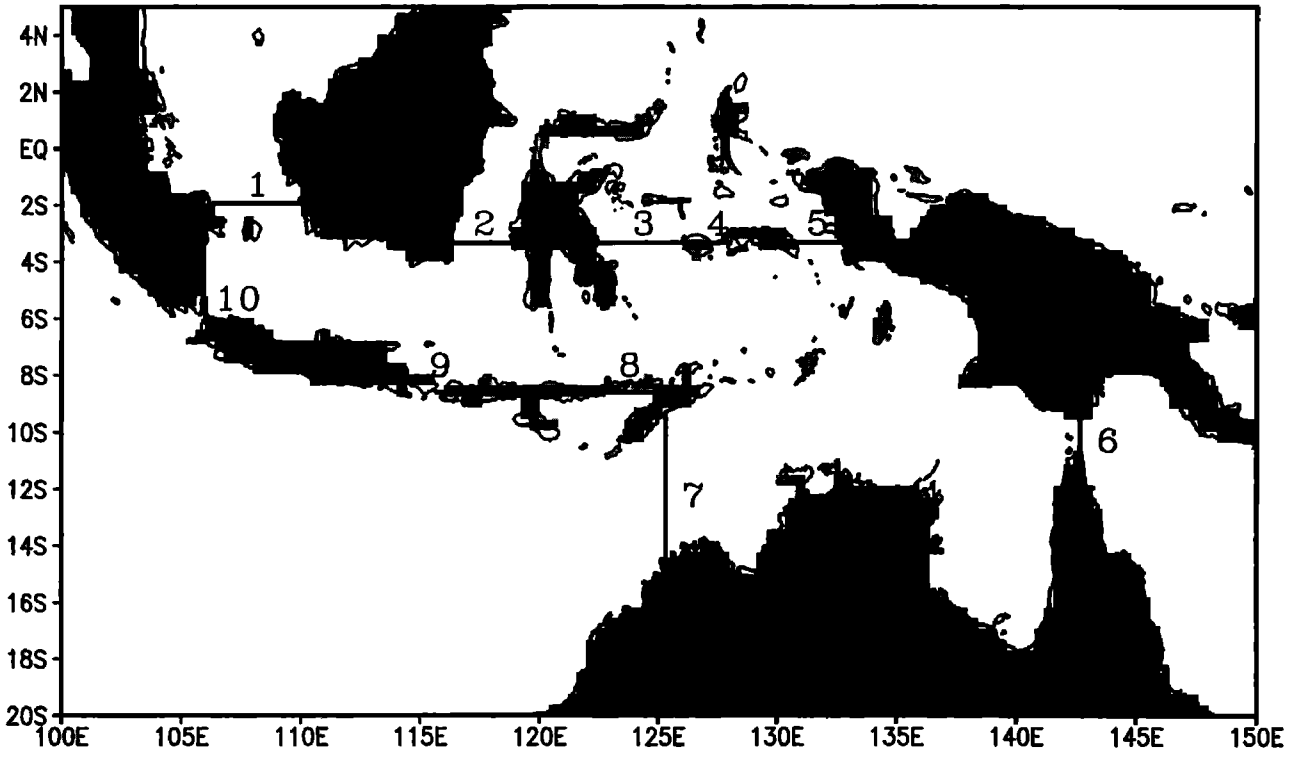

Figure 4. Model geometry and section locations. Model land points are shaded, and the sections where transport calculations were made are shown. The numbers correspond to those in Table 1.

The POCM velocity fields were used to compute transport into and out of the Indonesian seas. Velocity was sampled along specific transects (Figure 4), and the normal component of flow along these sections was integrated from surface to bottom (model values in each grid cell were summed along each track).

All transport calculations were made along sections south of the equator. The input of water to the Indonesian seas was measured along five zonal sections between 2° S and 3° S, and through a meridional section along 142° E. Output was measured along four sections. All values are summarized in Table 1.

Section 1 is the strait between Sumatra and Kalimantan, referred to here as the Karimata Strait. In the model resolution this strait is 22 km^2 in cross-sectional area, 50 m deep, and slightly more than 400 km wide. The model-derived velocity through this section is about 6 cm s^{-1} in the mean, but exhibits a large seasonal fluctuation on the western side (along Sumatra). The western meridional velocity is about 20 cm s^{-1} toward the north in July and 20 cm s^{-1} toward the south in January. This velocity results in a northward transport of 1.2 Sv in July, a southward transport of 4.0 Sv in January, and a long-term mean of 0.70 Sv toward the south (into the Indonesian seas).

Section 2 runs between Kalimantan and Sulawesi (the Makassar Strait). This strait is about 265 km wide and 500 m deep (more shallow on the western side of the strait), with a cross section of 56 km^2. Velocity through this section is northward on the western side (about 25 cm s^{-1} in December and January) and southward on the western side along the coast of Sulawesi (about 25 cm s^{-1} in June through August). Transport through the section averages 2.13 Sv toward the south (during model years 1987 through 1995), with peaks of 4 to 6 Sv during boreal spring and summer and reversal (up to 4 Sv toward the north) in January. This transport is exactly out of phase with flow in the Karimata Strait (which is southward in January). This is a result of

Table 1. Model Sections for Transport Calculations

No.	Section	Depth, m	Area, km^2	Transport, Sv
1	Karimata Strait	50	22	-0.70
2	Makassar Strait	510	56	-2.13
3	Molucca Strait	4500	1432	-3.44
4	Manipa Strait	710	98	0.04
5	Ceram Strait	1335	195	0.18
6	Torres Strait	50	15	-1.37
7	Timor Strait	1335	223	-0.10
8	Ombai Strait	1000	196	-6.95
9	Lombok Strait	185	30	0.00
10	Sunda Strait	50	7	-0.32

All values are based on the model configuration; negative values indicate southward or westward flow. The section numbers correspond to those in Figure 4.

flow around the island of Kalimantan, which is clockwise around the island in austral summer and counter clockwise in austral winter (Figure 3).

Section 3 is the most open, and most of the water that goes into the Indonesian seas enters through it (in the model). This section is the Molucca Strait, and it is between Sulawesi and Buru. The cross sectional area along 3° S in the model is 1432 km^2 (396 km wide and 4500 m deep). Velocity through this strait is mostly in the top 200 m and has more of an interannual signal than annual. Mean flow is about 5 cm s^{-1} toward the south, but in early 1987, 1992, and 1993 it is northward at 15 cm s^{-1}. Flow is generally stronger on the western side of this strait. The mean transport is 3.44 Sv toward the south.

The last two sections along 3° S, sections 4 and 5, are small in the model, and the transport is low. The Manipa Strait, between the islands of Buru and Ceram, has a cross sectional area of 98 km^2. In the model the strait is about 44 km wide and 700 m deep. The mean transport is about 0.04 Sv northward. The other strait is between Ceram and New Guinea, the Ceram Strait. This strait is only 15 km^2 in the model, and the transport is 0.18 Sv toward the north.

The final inflow section, section 6, is along the Torres Strait, between New Guinea and Australia. Even though the strait is very shallow (50 m) and narrow (132 km), the velocity can be quite large (30 cm s^{-1}), and the mean transport is 1.37 Sv toward the west. This signal also has a large seasonal component, with 2 Sv toward the east in January and 4 Sv toward the west in July. Figure 5 shows the transport time series as computed from the model. This flow must be considered unrealistic due to the exaggerated model topography.

The sum of these six sections matches the total outflow from the Indonesian seas (hereinafter referred to as the throughflow). The components of the throughflow are broken down into four straits. The Lombok Strait, between Lombok and Bali, is resolved by only one model grid point, and consequently there is no flow

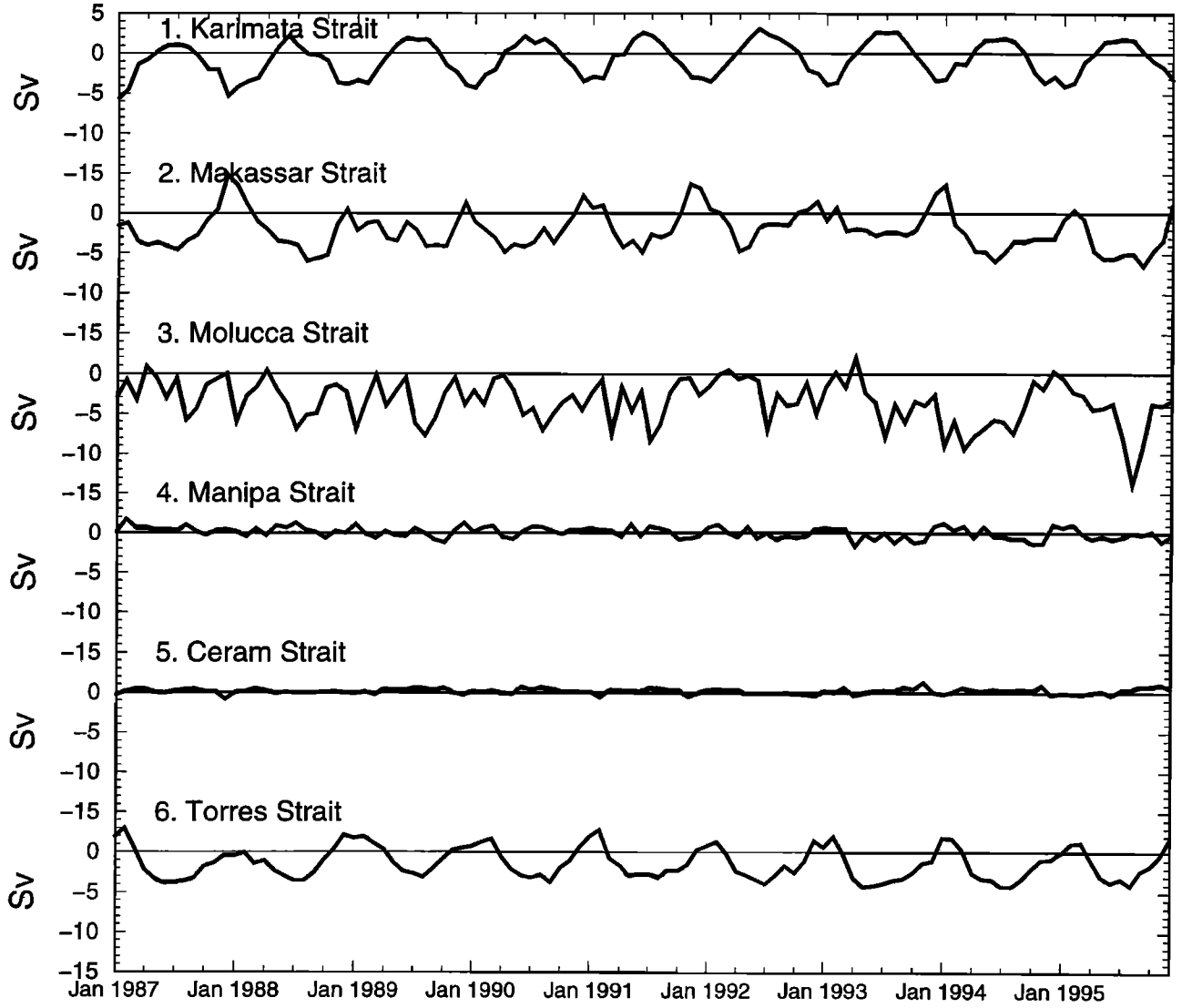

Figure 5. Inflow transports in Sverdrups. Section locations are given in Table 1. Negative values indicate southward or westward flow (i.e., flow into the Indonesian seas.

through it. The major contribution to the throughflow is through the Ombai Strait (section 8) between Timor and Flores. The strait is only 196 km^2 in cross section, but the velocity is large (about 50 cm s^{-1}). The mean transport is 6.95 Sv toward the south.

The remaining two straits, between Australia and Timor, and the Sunda Strait (between Sumatra and Java), account for less than 0.5 Sv. In the case of the Sunda Strait, it is because the strait is very small (7 km^2). In the case of the Timor Sea, the transport is low due to a large seasonal signal in the velocity, which reverses direction. In January it is toward the east, and in April it is toward the west. The outflow transports are shown in Figure 6.

The total throughflow is computed as a sum between sections 7 through 10 (although in the model, section 9 has zero transport). The resulting throughflow has a mean of 7.4 Sv over the 9-year model run (1987 through 1995). Figure 7 shows the model-derived transport and its annual harmonic. The throughflow was also measured using model velocities normal to a section from Java to Australia, with little difference between this section and the sum of the transports from the aforementioned straits. In order for the transport to change appreciably from one section to the next, sea level would need to change by an unrealistic amount. Therefore storage of water in this region does not seem to be an issue on these timescales.

This net throughflow agrees quite well with the modeling results of *Inoue and Welsh* [1993] and *Masumoto and Yamagata* [1996], and with the observations of *Meyers* [1996]. The seasonal cycle, similar to observations, shows minimum transport during January and February and maximum during July and August [*Fieux et al.*, 1994, 1996]. It should be noted that a relatively large fraction of the nonseasonal variability in throughflow transport is of short timescale. Maximum throughflow transport of 15 Sv occurs during the La Niña years (e.g., 1988, 1994). The minimum transport occurs during El Niño (e.g., 1991, 1992, 1993), with weak transport into the Indonesian seas. This is consistent with the theoretical discussion by *Clarke and Liu* [1994]. During El Niño years, sea level decreases in the warm pool, and thereby the pressure difference between the Pacific and Indian Ocean is diminished, along with the throughflow. During the La Niña years 1988-1989, the reverse case occurs. These results are also seen in the XBT data of *Meyers et al.* [1995].

2.3. Ekman and Geostrophic Transports

A calculation of Ekman transport through a section from Java to Australia using the 10 m ECMWF winds from 1987 through 1997 (the same winds used to force the POCM) shows that the ageostrophic portion of the ITF transport is not insignificant (1.8 Sv on average (Figure 8)). It has a strong seasonal signal, sometimes as large as 5 Sv. Interannual variations of the Ekman component of model ITF are no larger than the noise of month-to-month variations. The model ITF, after subtraction of the Ekman transport through the section, is geostrophic to within the errors of transport computation on the model grid. For this study, indexing schemes are derived using both the total model ITF transport and the model transport with the Ekman transport removed (model "geostrophic" transport).

Since the model ITF transport is nearly geostrophic, a simple indexing scheme would be to use the difference in sea level on either side of the Indo-Australian Basin (e.g., difference in sea level along south coast of Java and the northwest coast of Australia). Figure 9 shows how the sea level in the model changes along both these coastlines, making it difficult to find an appropriate lo-

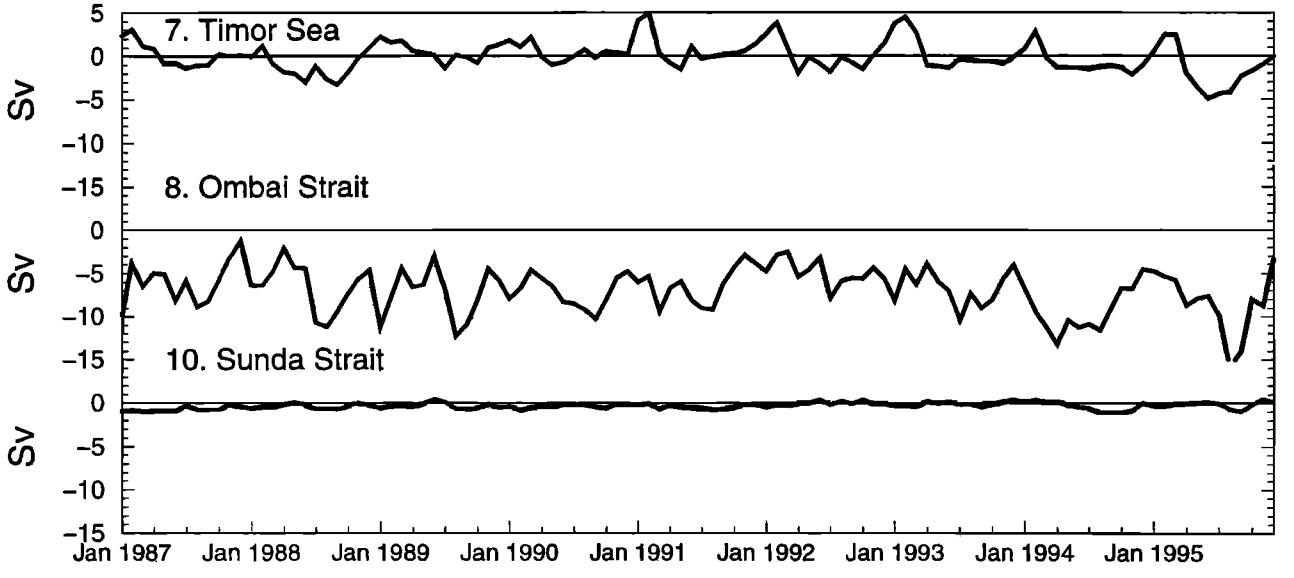

Figure 6. Outflow transports in Sverdrups. Section locations are given in Table 1. Negative values indicate southward or westward flow (i.e., flow out of the Indonesian seas.

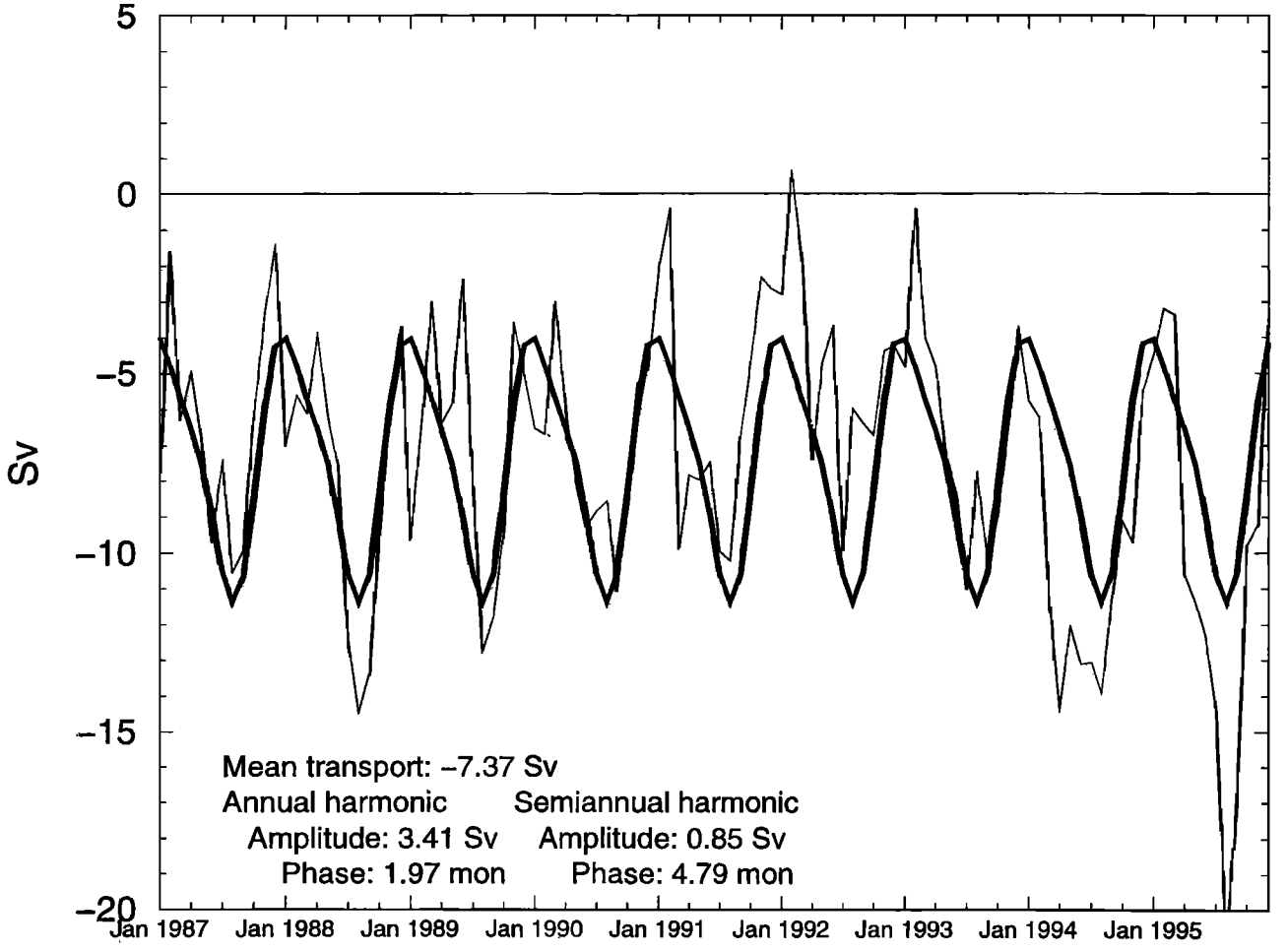

Figure 7. Monthly average POCM ITF transport (thin line). Negative values indicate transport from the Indo-Australian Basin into the Indian Ocean. The heavy line is the annual and semiannual harmonic for the 9 years shown.

cation to compute a geostrophic calculation. In addition, tide gauge records are not extensively available, particularly along the southern Sumatra-Java coast.

In the model, at monthly mean intervals, the sea level anomalies along the northwest coast of Australia (from 20° S, 120° E, to 11° S, 135° E) are coherent. Generally, sea level is higher than average in May-June and lower than average in December-February. This model sea level annual cycle, though, lags the observations by 2 months [*Wyrtki*, 1987]. This is due to either problems with the surface forcing in this region [*Stammer et al.*, 1996] or a problem with the model physics on the broad, shallow shelf along the northwest coast of Australia. Since the shelf is shallow, wind effects would be more dominant in this region.

The signal from the southern Indonesian coastline, taken from 106° E, 7° S to 121° E, 10° S, is less coherent from east to west but still shows a strong annual cycle. In this case the annual cycle is out of phase with that of the Australian coastal sea level. Higher than average sea level appears in February, and lower than average occurs in August.

POCM mean sea level anomalies along each coastline exhibit strong annual and semiannual signals (Figure 10). These two frequencies dominate the northwestern Australian sea level signal. The Indonesian sea level signal also has significant peaks at interannual (48 and 18 month) periods, with less energy in the annual and semiannual frequencies. This agrees with the hypothesis of *Wyrtki* [1987] as well as the work by *Clarke and Liu* [1994].

3. Sea Level Index Development

Due to insufficient observations along the coastline bordering the Indo-Australian Basin, and the difficulty of determining an appropriate location for a geostrophic calculation based on sea level difference, a different approach is suggested here. The model results are used

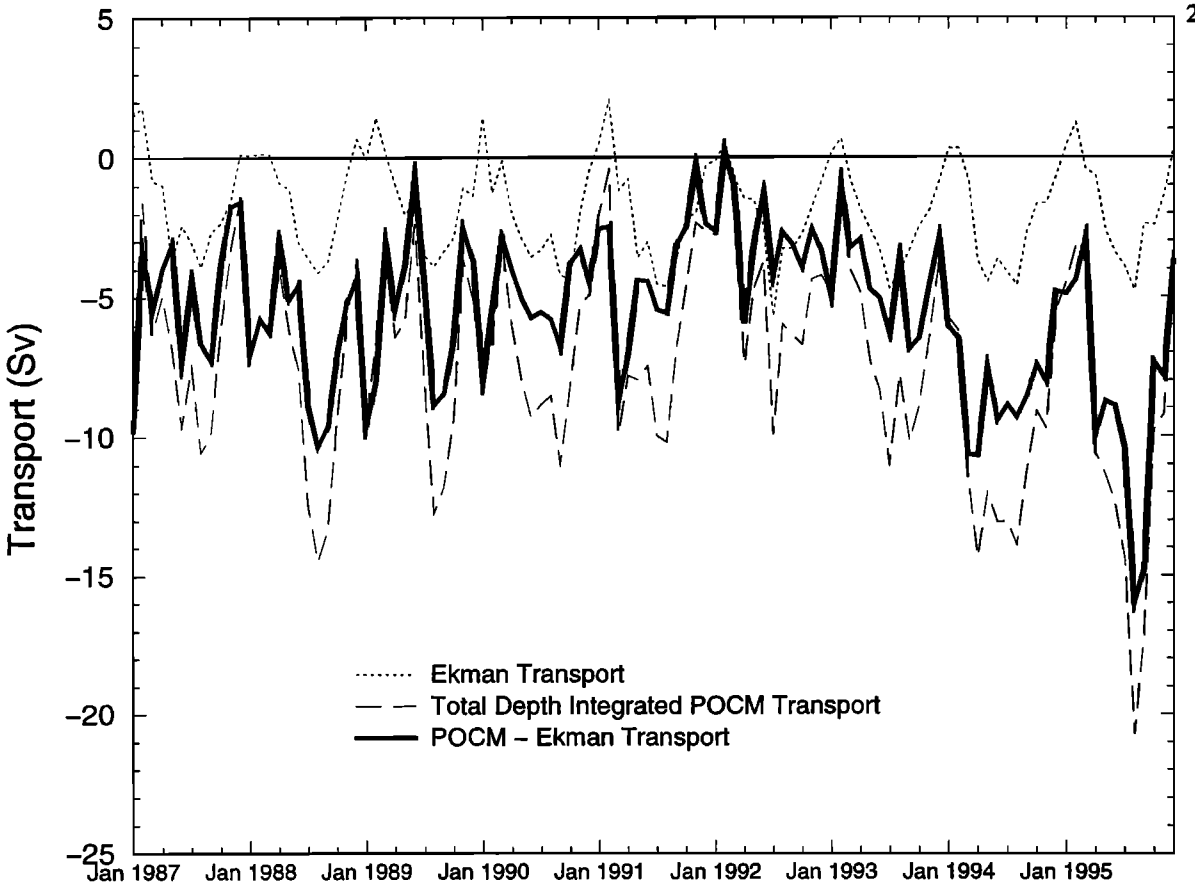

Figure 8. The 10 m ECMWF winds from 1987 through 1995 were used to compute Ekman transport (dotted line). The total model depth-integrated transport is given by the dashed line, and the difference between the two is the solid line.

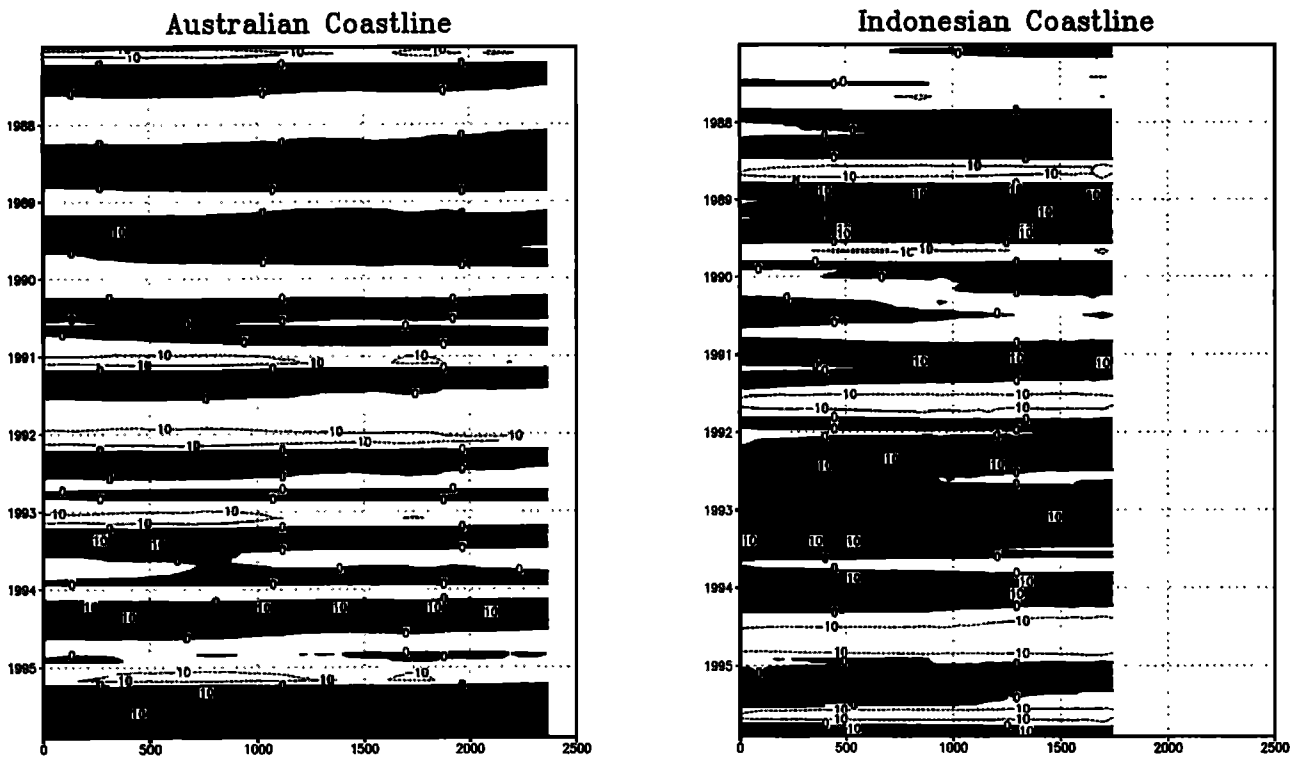

Figure 9. Sea level anomalies (in centimeters) from the model, as measured along the coast. The abscissa is distance in kilometers along the coast. The left panel is measured along the northwestern Australian coast, from 120° E, 20° S eastward. The right panel is along the southern coasts of the Sunda Islands from 106° E, 7° S eastward. Sea level higher than average is shaded.

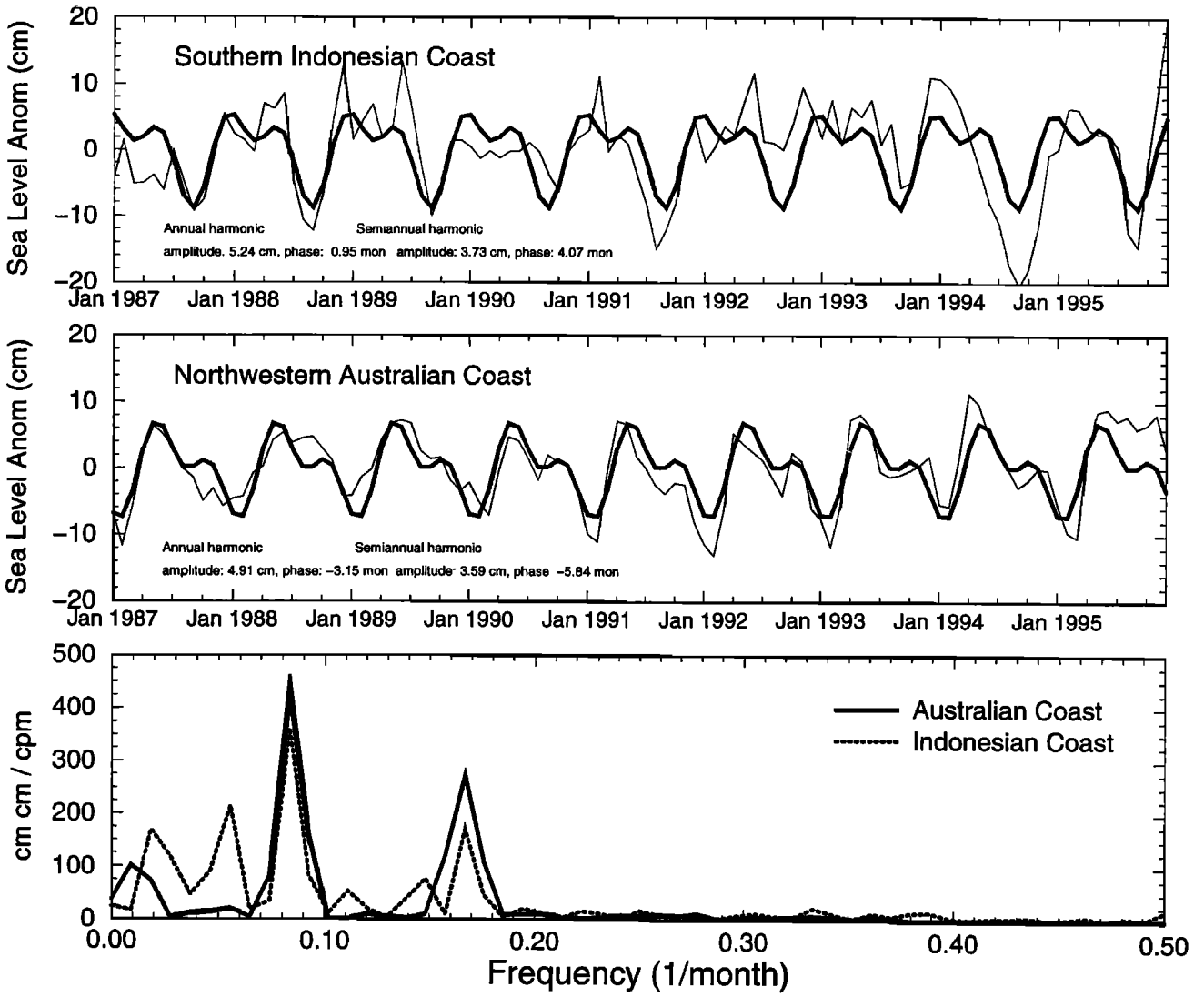

Figure 10. Mean POCM sea level anomalies (top) along the southern Indonesian coastline and (middle) along the northwestern Australian coast (thin lines). These are means of the sections in Figure 9. The annual and semiannual harmonic of each signal are also shown (thick line). (bottom) Power spectral density of each time series.

to determine regions affecting the Pacific-Indian Ocean pressure difference. Sea level at these regions is then combined and fit to the model throughflow variations. If the model physics is sufficient, observed sea level at these same regions would combine in a similar way to index the observed ITF variability.

First, large-scale pressure differences between the Pacific Ocean and Indian Ocean are estimated using the *Wyrtki* [1987] approach. Mean sea level anomalies over four model grid points were computed at two locations (131.0° E, 11.3° S, corresponding to Darwin, and 126.6° E, 7.0° N, corresponding to Davao). The difference in model free surface elevation between Davao and Darwin (Figure 11) is shown in Figure 12.

As noted earlier, the sea level anomalies at Darwin (northwestern Australia) lag the observed sea level anomalies (from tide gauge data) by 2 months. The observed annual cycle has sea level higher than average in February and March, and lower than average during July and August. The model maximum anomaly is during May and June, while the minimum is during January and February. *Stammer et al.* [1996] conjecture that the ECMWF wind forcing accounts for this lag at Darwin.

As in the *Wyrtki* [1987] study, this difference matches well with the annual cycle of throughflow transport but misses some of the larger interannual components. The long-term sea level difference from the model is uncorre-

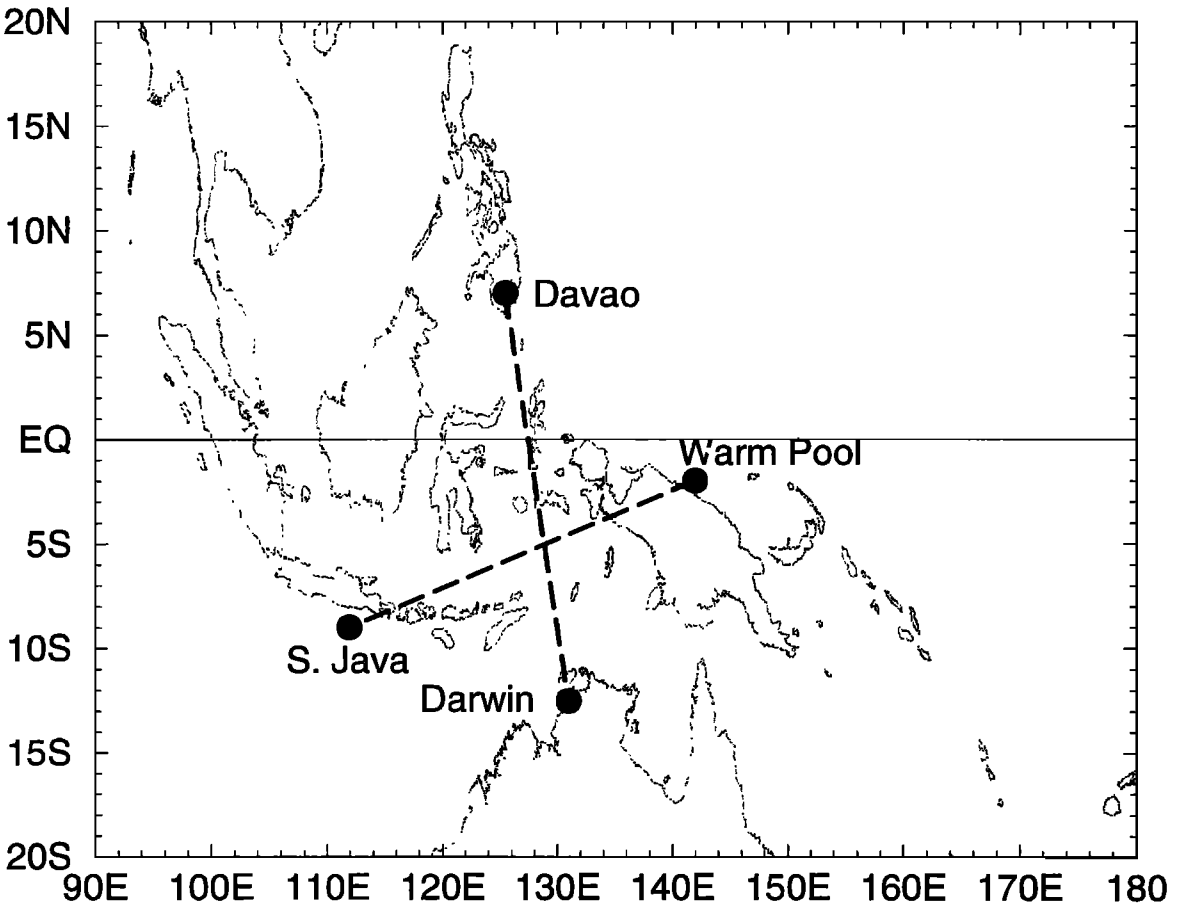

Figure 11. Australasian regional map indicating the locations of POCM free surface height anomalies used in developing the model transport index.

lated to both the model total and geostrophic transport (correlation of 0.24 and 0.14, respectively). In an attempt to address the interannual variations in the ITF, the difference in sea level between the Pacific warm pool and along the Indonesian coast in the Indian Ocean were examined, following *Clarke and Liu* [1994].

Mean sea level anomalies were computed over four model grid points at a region south of Java and in the Pacific warm pool (Figure 11). This difference picks up the larger interannual changes, in agreement with *Clarke and Liu* [1994]. The model sea level difference between these two locations has a correlation coefficient of 0.60 to the model geostrophic flow.

To get a complete picture, the sea level index of the ITF variability developed here incorporates all four locations: the warm pool and Davao in the Pacific, and Darwin and along the southern coast of Indonesia in the Indian Ocean.

Sea level from the POCM at the two tide gauge sites (Davao and Darwin) was averaged over four model grid points. For the south Java and Pacific warm pool indices, sea level was averaged over a larger region. In the warm pool, 200 model grid points were used, corresponding to a region 9° by 4° along the eastern side of New Guinea. For the South Java signal, a mean was computed over 40 model grid points, a strip 8° by 2°, along the South Java coast.

Sea level anomalies from the four locations described above were fit to the model ITF transport anomalies using a multiple linear regression (MLR) technique [*Chelton,* 1983]. The model sea level anomalies at these four locations were normalized to have unit variance, then fit to the model transport variations. Anomalies were fit to ITF variations, since any application with observed or remotely sensed data would only be able to estimate variations. The procedure was carried out using both the total model transport and "geostrophic" model transport at various lags.

The basis functions, i.e., normalized model sea level anomalies at the four locations, are shown in Figure

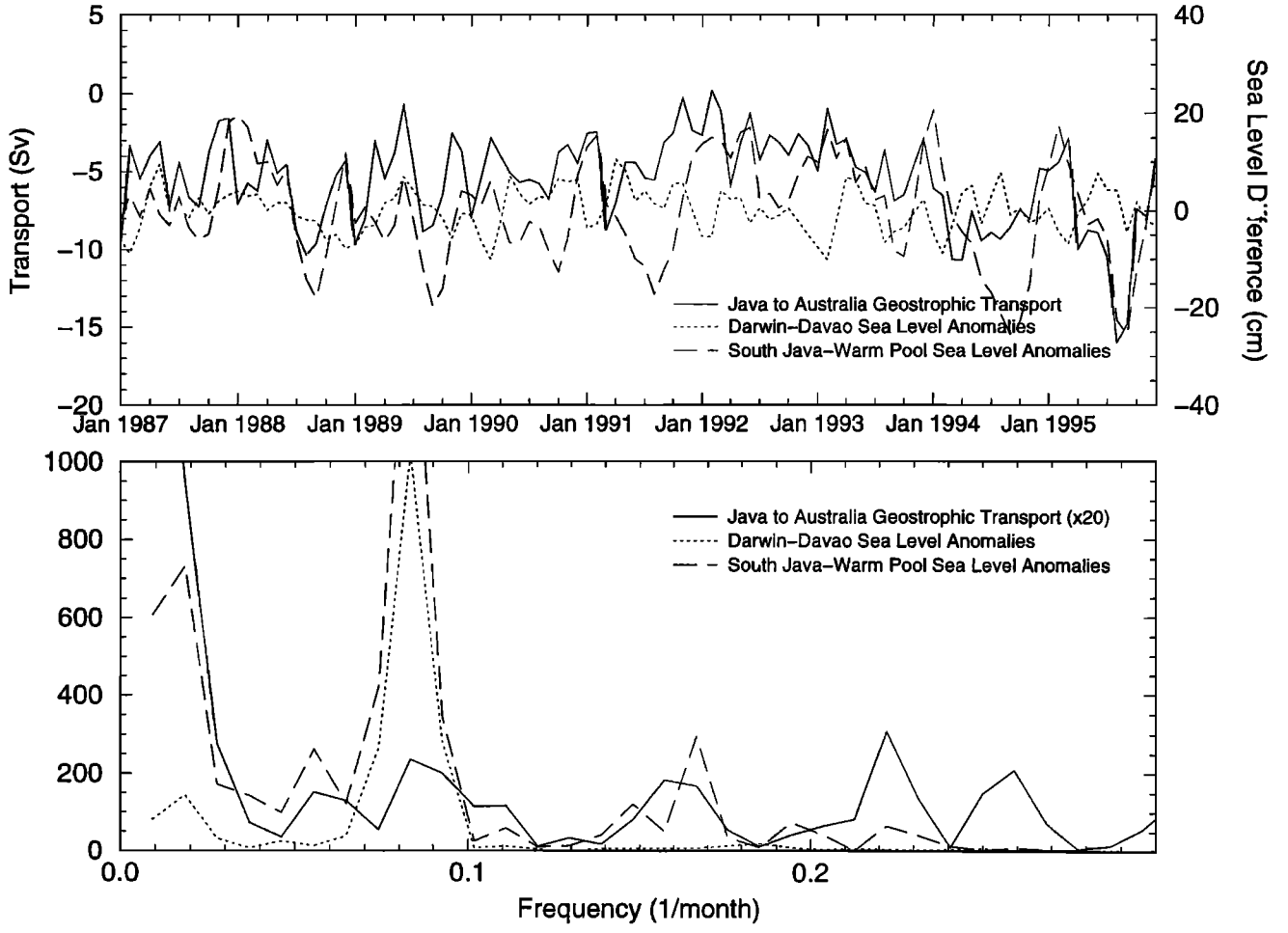

Figure 12. (top) Model transport taken along a section from Java to Australia, with the Ekman component subtracted off (solid line). The sea level anomalies (dashed and dotted lines) are taken from the model as well, from locations shown in Figure 11. The transport scale (Sverdrups) is given on the right-hand axis, while the sea level difference (centimeters) is given on the left side. (bottom) Power spectral density of the time series in the upper panel.

13. In the case where Ekman transport is removed, the warm pool and south Java signals are combined as before. Sea level anomalies at south Java (weighted by 1.35) minus the warm pool (weighted by 0.91) give large ITF anomalies (Pacific to Indian Ocean transport is a negative number), as do those at Darwin (weighted by 0.32) minus Davao (weighted by 1.32).

$$V'_{\mathrm{ITF}} = 1.35\ \eta'_{\mathrm{SJ}} - 0.91\ \eta'_{\mathrm{WP}} + 0.32\ \eta'_{\mathrm{DAR}} - 1.32\ \eta'_{\mathrm{DAV}} \quad (1)$$

where

V'_{ITF} depth-integrated ITF transport anomalies from the POCM with Ekman flow removed;

η'_{SJ} sea level anomalies averaged over a region south of Java, normalized to have unit variance;

η'_{WP} sea level anomalies averaged over a region in the western Pacific warm pool, normalized to have unit variance;

η'_{DAR} sea level anomalies at Darwin, northwest Australia, normalized to have unit variance;

η'_{DAV} sea level anomalies at Davao, Philippines, normalized to have unit variance.

In the case where Ekman transport is included, the warm pool sea level signal is again weighted by −0.91, but the South Java signal is weighted more heavily (2.40). The Davao signal is also weighted close to the

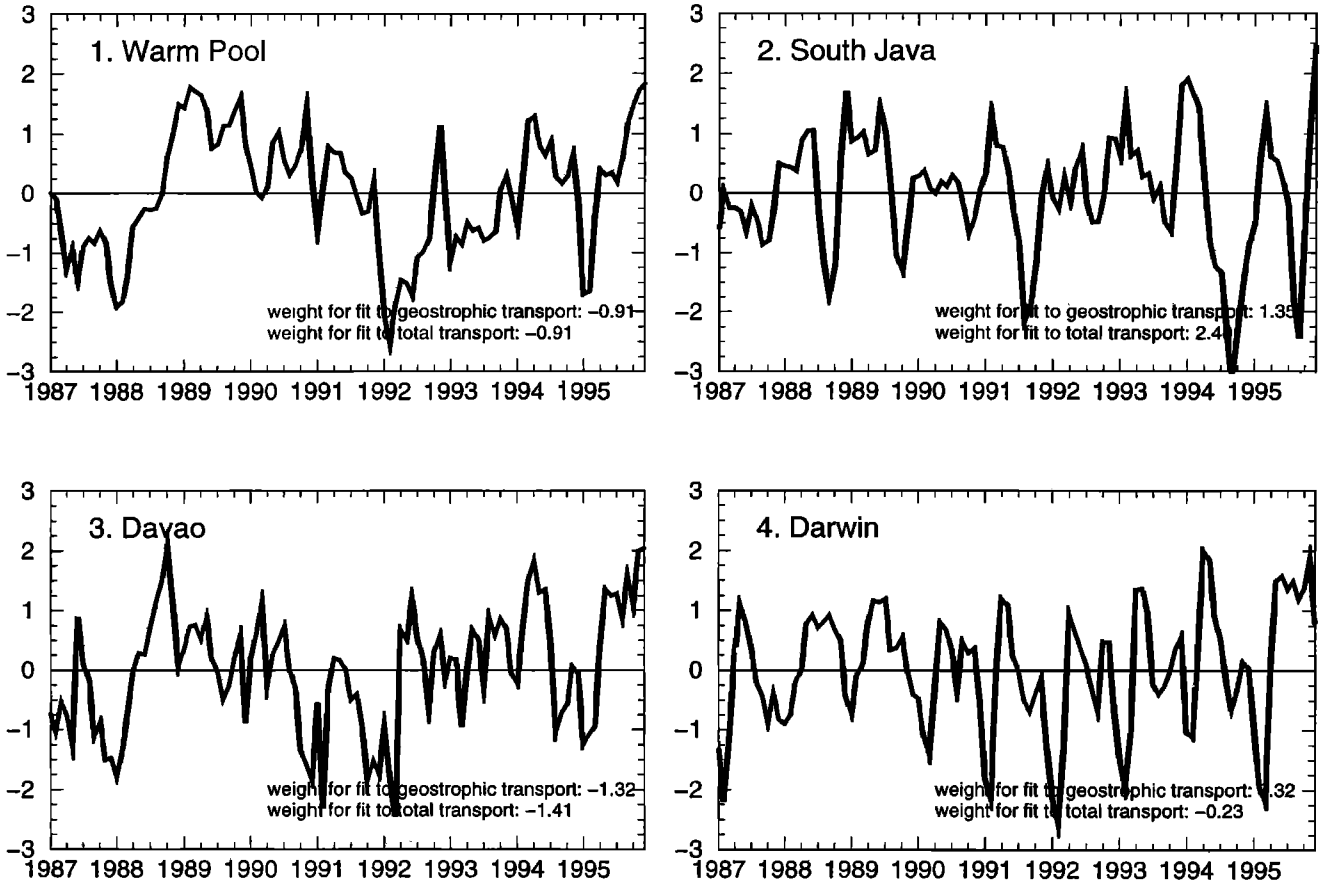

Figure 13. POCM sea level signals for the regions identified in Figure 11. The signals have been normalized to unit variance, and the weights for the signals are given in each panel.

same (−1.41) while the Darwin signal weight is reduced to −0.23. The index, then, can be represented as

$$V'_{\mathrm{ITF}} = 2.4\ \eta'_{\mathrm{SJ}} - 0.91\ \eta'_{\mathrm{WP}} - 0.23\ \eta'_{\mathrm{DAR}} - 1.41\ \eta'_{\mathrm{DAV}} \quad (2)$$

The signals from the warm pool are consistent with ENSO activity. The large increase in throughflow in 1995, however, seems to be reflected more in the south Java signal, suggestive of an Indian Ocean source.

Sea level anomalies south of Java have a mixture of interannual and annual periods. This region is under the influence of seasonally reversing monsoon winds. During boreal summer and fall, there are strong southeasterlies, which cause offshore flow from Java. This would be reflected in higher sea levels. There are also semiannual Kelvin waves that propagate along the coast, forced by the monsoon transition in the equatorial Indian Ocean and the resulting Wyrtki jet [*Gill*, 1982].

The multiple linear regression fit of these sea level anomalies to the total and geostrophic model transport anomalies are shown in Figure 14. The correlation coefficient R of the index and model ITF transport is 0.83. For the fit to the model transport with Ekman transport removed, the correlation coefficient is 0.71. Both of these numbers, as well as the R^2 values, are significant at the 95% level. Most of the unexplained variance seems to occur at higher frequency. It could be expected that with more stations (basis functions) an even higher correlation could be achieved.

Finally, the sea level anomalies from the TOPEX altimeter data were used in equation (2). Ideally, the result should be compared to observed throughflow transports. Since there are insufficient records for such a comparison, the result is compared to the POCM transport anomalies. Figure 15 shows the index from TOPEX sea level and the model transport. The two time series have a correlation of 0.78. The 5-day TOPEX data were averaged to monthly mean to compare with the POCM data, but Figure 15 shows the raw data.

4. Discussion and Future Work

The first objective of this work was to identify appropriate processes important for controlling ITF trans-

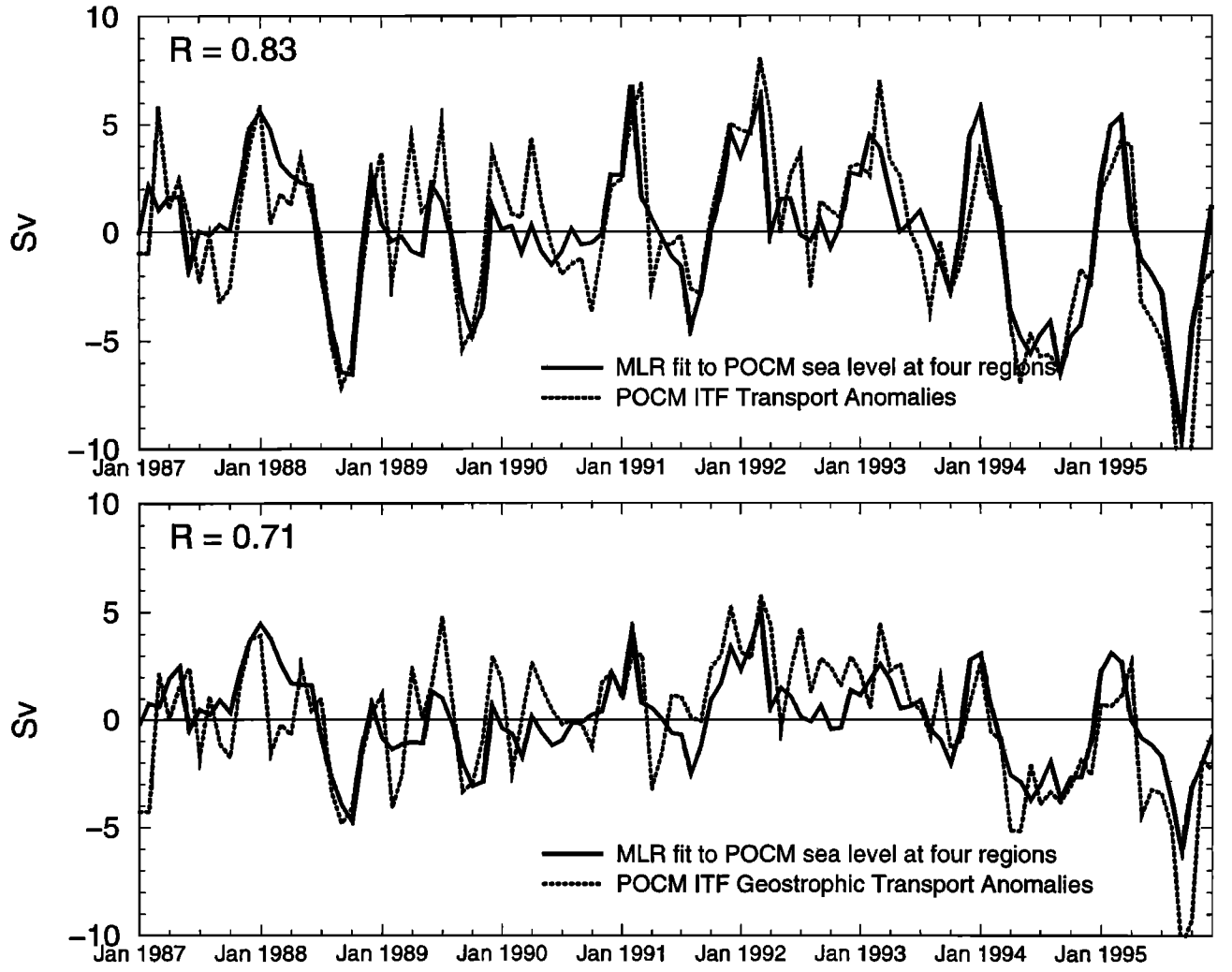

Figure 14. Monthly average POCM transport anomalies compared to the model sea level index described in the text: (top) the fit to the total model ITF transport anomalies, and (bottom) the fit to the model transport with Ekman transport removed. Negative values reflect flow from the Pacific to the Indian Ocean.

port variations. Comparison of the POCM data to TOPEX altimetry shows that the large-scale pressure forcing (reflected in sea level variations) acts on different timescales in different regions. The interannual fluctuations of the ITF appear to be controlled on the Pacific Ocean side. Annual fluctuations are controlled both by warm pool variability as well as Indian Ocean processes. An optimal indexing scheme therefore would require data on both sides of the ITF region.

The model throughflow has an annual harmonic with a peak in boreal summer (11 Sv) and a minimum in boreal winter (4 Sv). Fluctuations on interannual timescales show the ITF to increase during El Niño (e.g., 1986-1987, 1991, 1992, 1993) and decrease during La Niña (e.g., 1988-1989). The annual cycle can be explained by direct forcing of the monsoons, which are in the direction of the throughflow during July and August and oppose it in December and January. The interannual variability is a response to the large-scale pressure changes associated with ENSO. During El Niño the sea level in the western Pacific is reduced, and likewise the pressure gradient from the Pacific to the Indian Ocean is reduced. The reverse is true during La Niña.

It was demonstrated, using both the ECMWF wind field (over a different time period) and the model results, that the directly wind-driven component of the throughflow was not always negligible. The long-term mean is almost 1.8 Sv, but the annual variations can contribute as much as 5 Sv to the ITF during the boreal summer.

Nevertheless, it has been shown that sea level signals over a few well-chosen regions can reasonably index the

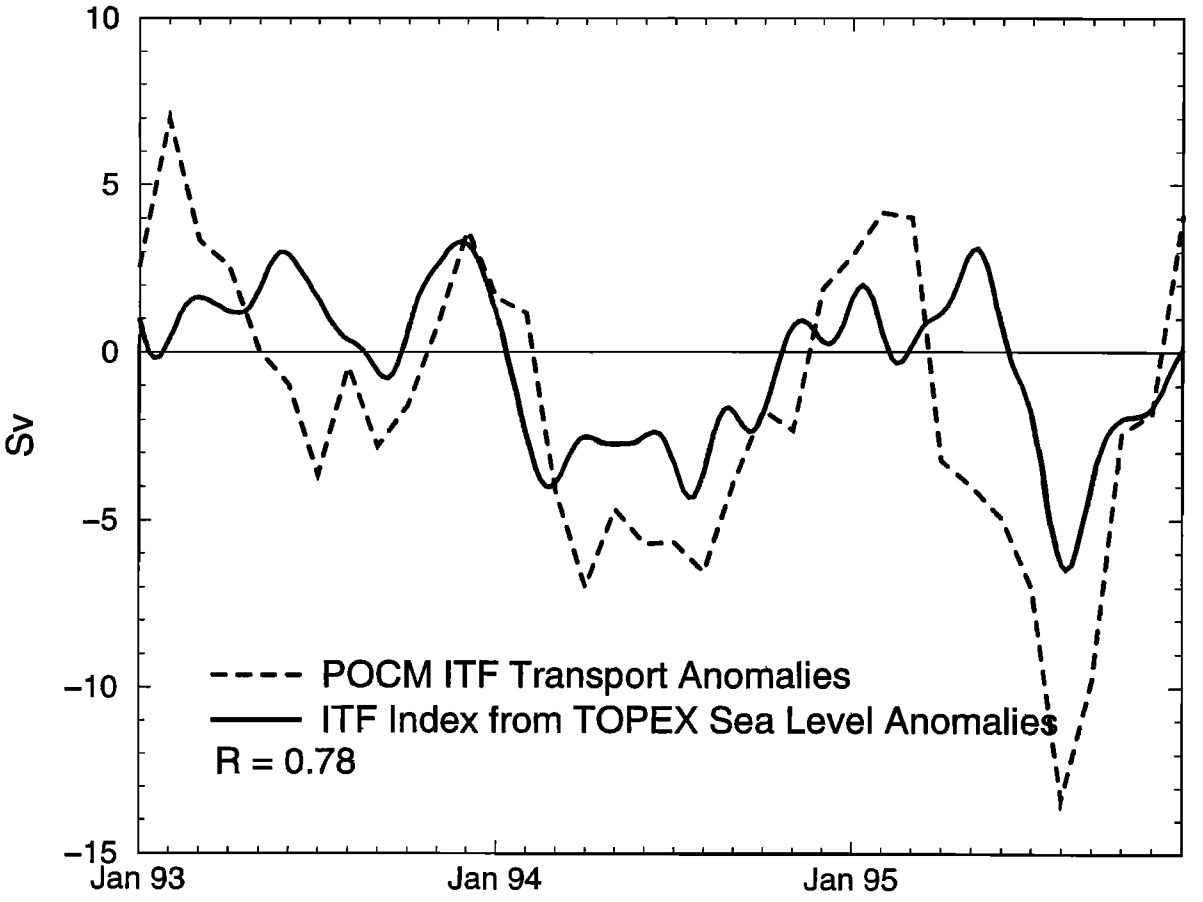

Figure 15. ITF index based on TOPEX sea level anomalies. The solid line shows the index and the dotted line shows the model ITF transport variations. The TOPEX data are displayed at 5-day intervals while the model ITF is monthly mean.

ITF transport. Using just a geostrophic approximation to the ITF is not sufficient, due to the complex dynamics involved on the Indonesian side of the region. Sea level on this side does, however, have more of an interannual signal than the Australian side. Consequently, an index based on four regions is weighted most by the Indonesian and warm pool regions and less heavily by the Davao-Darwin sea level difference [*Wyrtki,* 1987]. A better analysis of factors controlling the throughflow, and an expansion of the above outlined MLR technique, would result in a larger correlation.

Addition of in situ coastal sea level (where altimetric sea level has high noise levels due to tide model problems) may be desirable to obtain a better estimator. It may also be advisable to extend the index to include variable regional wind stress, if reliable data can be routinely obtained. A plan for calibration and verification of the ITF sea level index against direct in situ volume transport measurements must be developed to gain sufficient confidence in the utility of the index.

Acknowledgments. The authors would like to thank Bert Semtner for generously providing the model data, and for the professional and frequent assistance of Robin Tokmakian in answering numerous questions regarding the model code. The TOPEX data were provided by David Stone, and tide gauge data were provided by the UH Sea Level Center. The skillful technical assistance of Sharon DeCarlo aided in the computations and generation of figures. This work was supported by JPL contract 958120 (TOPEX/POSEIDON) and NFS grant OCE-9024452.

References

Barnier, B., L. Siefridt, and P. Marchesiello, Thermal forcing for a global ocean circulation model using a three year climatology of ECMWF analyses, *J. Mar. Sys., 6,* 363-380, 1985.

Chelton, D. B., Effects of sampling errors in statistical estimation, *Deep Sea Res. Part I, 30,* 1,083-1,103, 1983.

Clarke, A. J., and X. Liu, Interannual sea level in the northern and eastern Indian Ocean, *J. Phys. Oceanogr., 24,* 1,224-1,235, 1994.

Ffield, A., and A. L. Gordon, Vertical mixing in the Indonesian thermocline, *J. Phys. Oceanogr., 22,* 184-195, 1992.

Fieux, M., C. Andrie, P. Delecluse, A. G. Ilahude, A. Kartavseff, F. Mantisi, R. Molcard, and J. C. Swallow, Measurements within the Pacific-Indian Oceans throughflow region, *Deep Sea Res. Part I, 41,* 1,091-1,130, 1994.

Fieux, M., R. Molcard, and A. G. Ilahude, Geostrophic transport of the Pacific-Indian Oceans throughflow, *J. Geophys. Res., 101,* 12,421-12,432, 1996.

Fu, L. L., E. J. Christensen, C. A. Yamarone, M. Lefebvre, Y. Menard, M. Dorrer, and P. Escudier, TOPEX/ PO-

SEIDON mission overview, *J. Geophys. Res., 99,* 24,369-24,382, 1994.

Gill, A., *Atmosphere-Ocean Dynamics*, 662 pp., Academic, San Diego, Calif., 1982.

Godfrey, J. S., The effect of the Indonesian throughflow on ocean circulation and heat exchange with the atmosphere: A review, *J. Geophys. Res., 101,* 12,217-12,238, 1996.

Inoue, M., and S. E. Welsh, Modeling seasonal variability in the wind-driven upper-layer circulation in the Indo-Pacific region, *J. Phys. Oceanogr., 23,* 1,411-1,436, 1993.

Kindle, J., G. W. Heburn, and R. C. Rhodes, An estimate of the Pacific to Indian Ocean throughflow from a global numerical model, in *Further Progress in Equatorial Oceanography,* edited by E. J. Katz and J. M. Witte, pp. 317-321, Nova Univ. Press, Fort Lauderdale, Fla., 1987.

Kindle, J., H. Hurlburt, and J. Metzger, On the seasonal and interannual variability of the Pacific to Indian Ocean throughflow, in *Proceedings of the Western Pacific International Meeting and Workshop on TOGA COARE,* edited by J. Picaut, R. Lukas, and T. Delcroix, pp. 355-365, Centre ORSTOM de Nouméa, Nouméa, New Caledonia, 1989.

Levitus, S., Climatological atlas of the world ocean, *NOAA Prof. Pap. 13,* 173 pp., U. S. Govt. Print. Off., Washington, D. C., 1982.

Levitus, S., R. Burgett, and T. Boyer, World ocean atlas 1994, vol 3, Salinity, *NOAA Atlas NESDIS 3,* Natl. Oceanic and Atmos. Admin., Silver Spring, Md., 1994a.

Levitus, S., R. Burgett, and T. Boyer, World ocean atlas 1994, vol 4, Temperature, *NOAA Atlas NESDIS 4,* Natl. Oceanic and Atmos. Admin., Silver Spring, Md., 1994b.

Masumoto, Y., and T. Yamagata, Seasonal variations of the Indonesian throughflow in a general circulation model, *J. Geophys. Res., 101,* 12,287-12,293, 1996.

Meyers, G., Variation of Indonesian throughflow and El Niño-Southern Oscillation, *J. Geophys. Res., 101,* 12,255-12,264, 1996.

Meyers, G., R. J. Bailey, and A. P. Worby, Geostrophic transport of Indonesian throughflow, *Deep Sea Res. Part I, 42,* 1,163-1,174, 1997.

Mitchum, G., Comparison of TOPEX sea surface heights and tide gauge sea levels, *J. Geophys. Res., 99,* 24,541-24,554, 1994.

Molcard, R., M. Fieux, J. C. Swallow, A. G. Ilahude, and J. Banjarnahor, Low frequency variability of the currents in Indonesian channels (Savu-Roti and Roti-Ashmore reef), *Deep Sea Res. Part I, 41,* 1,643-1,661, 1994.

Murray, S. P., and D. Arief, Throughflow into the Indian Ocean through the Lombok Strait, January 1985 - January 1986, *Nature, 333,* 444-447, 1988.

Semtner, A. J., and R. M. Chervin, A simulation of the global ocean circulation with resolved eddies, *J. Geophys. Res., 93,* 15,502-15,522, 1988.

Semtner, A. J., and R. M. Chervin, Ocean general circulation from a global eddy-resolving model, *J. Geophys. Res., 97,* 5,493-5,550, 1992.

Stammer, D., R. Tokmakian, A. Semtner, and C. Wunsch, How well does a 1/4 degree global circulation model simulate large-scale oceanic observations?, *J. Geophys. Res., 101,* 25,779-25,811, 1996.

Tokmakian, R., Comparison of time series from two global models with tide-gauge data, *Geophys. Res. Lett.,* in press, 1996.

Wajsowicz, R. C., Flow of a western boundary current through multiple straits: An electrical circuit analogy for the Indonesian throughflow and archipelago, *J. Geophys. Res., 101,* 12,295-12,300, 1996.

Wyrtki, K., Physical oceanography of the southeast Asian waters, *NAGA Rep. 2,* 195 pp., Scripps Inst. of Oceanogr., La Jolla, Calif., 1961.

Wyrtki, K., Indonesian throughflow and the associated pressure gradient, *J. Geophys. Res., 92,* 12,941-12,946, 1987.

J. T. Potemra and R. Lukas, Department of Oceanography, University of Hawaii, 1000 Pope Road, Honolulu, HI 96822. (e-mail: jimp@soest.hawaii.edu; rlukas@soest.hawaii.edu)

G. T. Mitchum, Department of Marine Science, University of South Florida, 140 Seventh Avenue South, St. Petersburg, FL 33701. (e-mail: mitchum@marine.usf.edu)

(Received July 19, 1996; revised February 11, 1997; accepted June 13, 1997.)